MATERIALS CHEMISTRY
FRONTIERS

RESEARCH ARTICLE

View Article Online
View Journal | View Issue

Cite this: *Mater. Chem. Front.*, 2025, **9**, 3228

3D-Printable organic room-temperature phosphorescent elastomers based on *N*-ethylcarbazole derivatives

Yuxin Xiao,†[a] Haodong Sun,†[a] Yuanda Luo,[a] Zhuopeng Wu,[a] Shutong Zheng,[a] Jinsen Chen[a] and Tao Yu *[abc]

Received 14th July 2025,
Accepted 16th September 2025

DOI: 10.1039/d5qm00508f

rsc.li/frontiers-materials

Achieving stable, persistent room-temperature phosphorescence (RTP) within flexible and deformable elastomer matrices, particularly those that are amenable to advanced manufacturing techniques like 3D printing, is critical for developing future flexible sensors, yet it remains a significant challenge. Existing limitations often arise from quenching effects inherent to polymer motions, the poor solubility or dispersion of phosphors, and the difficulty in maintaining photophysical integrity under mechanical stress. Here, we address these challenges by introducing a versatile, generalisable approach to fabricate high-performance, 3D-printable RTP elastomers. *N*-Ethylcarbazole derivatives were developed as guest molecules doped into 3D-printable isobornyl acrylate (IBOA): benzyl acrylate (BA) resins. The resulting RTP elastomers exhibited exceptional photophysical properties under ambient atmospheric conditions. It is worthy of note that these elastomers retained their RTP properties consistently throughout both deformation under an external force and the fully recovered state and exhibited no observable alterations. This work provides a general, scalable solution for producing 3D printable RTP elastomers, establishing a foundation for exploring their applications in emerging fields such as flexible sensors and intelligent deformable structures.

Introduction

Recent advancements in room-temperature phosphorescent (RTP) materials have progressively shifted from optimizing the static luminescence properties to enabling functional and dynamic applications.[1–5] Through strategies such as molecular engineering, *e.g.* twisted conformation design and heavy-atom effect modulation,[6–11] host–guest doping,[12–17] and H-aggregation,[18–20] researchers have been able to control phosphorescence lifetimes and emission wavelengths in fields such as anti-counterfeiting,[21–23] bioimaging[24–27] and sensing.[28–30] However, current research focuses on rigid polymer films or molecular crystals, which suffer from poor elastic deformation capabilities and insufficient cycling stability, struggling to meet the demand for synchronized dynamic deformation and phosphorescent responses in emerging applications. The investigation of RTP elastomers holds significant importance in the field of smart materials as it integrates phosphorescence with elastomeric mechanical properties, offering innovative solutions for flexible wearable devices and dynamic stress-visualized sensing.

Therefore, the development of elastomeric RTP materials with high elasticity, recoverable deformation, and stable phosphorescence emission has become imperative. However, this field faces critical challenges in material design. On the one hand, phosphorescence emission requires rigid molecular frameworks to suppress the non-radiative transitions of triplet excitons, while the high deformability of elastomers demands substantial segmental mobility.[31–35] On the other hand, the reversible reconstruction of microstructures during dynamic deformation tends to disrupt the excited-state energy-transfer pathways of phosphorescent units, leading to luminescence decay.[36] Furthermore, achieving synchronized regulation of phosphorescence lifetime, emission wavelength, and mechanical responsiveness under complex stress remains a pivotal scientific bottleneck. Addressing these challenges necessitates the construction of multi-level molecular networks that harmonize rigidity and flexibility, coupled with unveiling of the fundamental principles governing photo-mechanical coupling

[a] *Frontiers Science Center for Flexible Electronics, Xi'an Institute of Flexible Electronics & Xi'an Institute of Biomedical Materials and Engineering, Northwestern Polytechnical University, 127 West Youyi Road, Xi'an 710072, China. E-mail: iamtyu@nwpu.edu.cn*
[b] *Key Laboratory of Flexible Electronics of Zhejiang Province, Ningbo Institute of Northwestern Polytechnical University, 218 Qingyi Road, Ningbo 315103, China*
[c] *Shenzhen Research Institute of Northwestern Polytechnical University, 45 Gaoxin Nanjiu Road, Shenzhen 518063, China*
† These authors made equal contributions to this article.

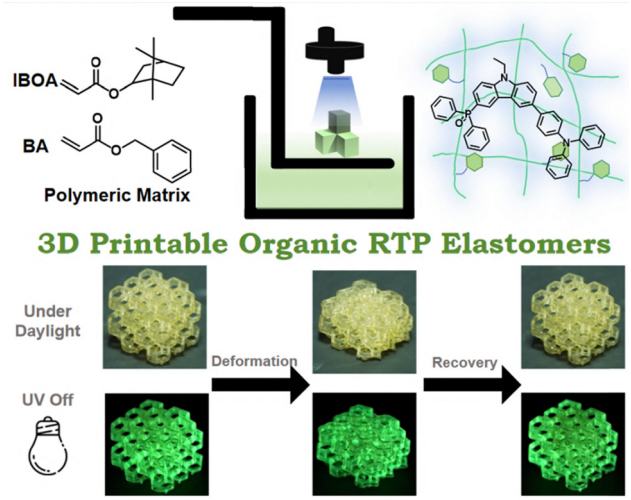

Fig. 1 Design of 3D-printable RTP elastomers based on *N*-ethylcarbazole derivatives.

mechanisms under external forces. Overcoming these limitations would advance intelligent luminescent materials from static properties to dynamic functionalities, offering substantial scientific value for next-generation adaptive optoelectronic systems.

In this work, we propose a universal strategy to design and prepare elastomeric RTP materials, as shown in Fig. 1. By integrating molecular engineering with a polymer matrix synergy strategy, we successfully developed novel materials that combine high elastic deformability (elongation at break exceeding 516%) with long-lived room-temperature phosphorescence (lifetime, $\tau \sim 412$ ms). Through targeted functionalization of carbazole derivatives, triphenylamine (TPA) and diphenylphosphine oxide (DPO) groups were introduced at the 3-/6-positions of an ethylcarbazole (EtCz) core, constructing three triplet-exciton-regulated compounds, namely, EtCzTPADPO, EtCzTPA, and EtCzDPO. These compounds were precisely dispersed into hydroxyethyl acrylate (HEA): acrylic acid (AA) resin and isobornyl acrylate (IBOA): benzyl acrylate (BA) elastomeric resin. Experimental results demonstrated that the TPA group significantly enhanced the intersystem crossing efficiency *via* intramolecular charge transfer (ICT). The P═O moiety in the DPO unit facilitated strong SOC, promoting ISC, as supported by the studies on phosphine oxide-containing systems. Besides, the n → π* transition associated with P═O further enhanced the SOC efficiency, contributing to rapid ISC and triplet-state population. Specifically, the interactions between the guest molecules and the polymer matrix played a pivotal role in suppressing non-radiative transitions to achieve efficient RTP.

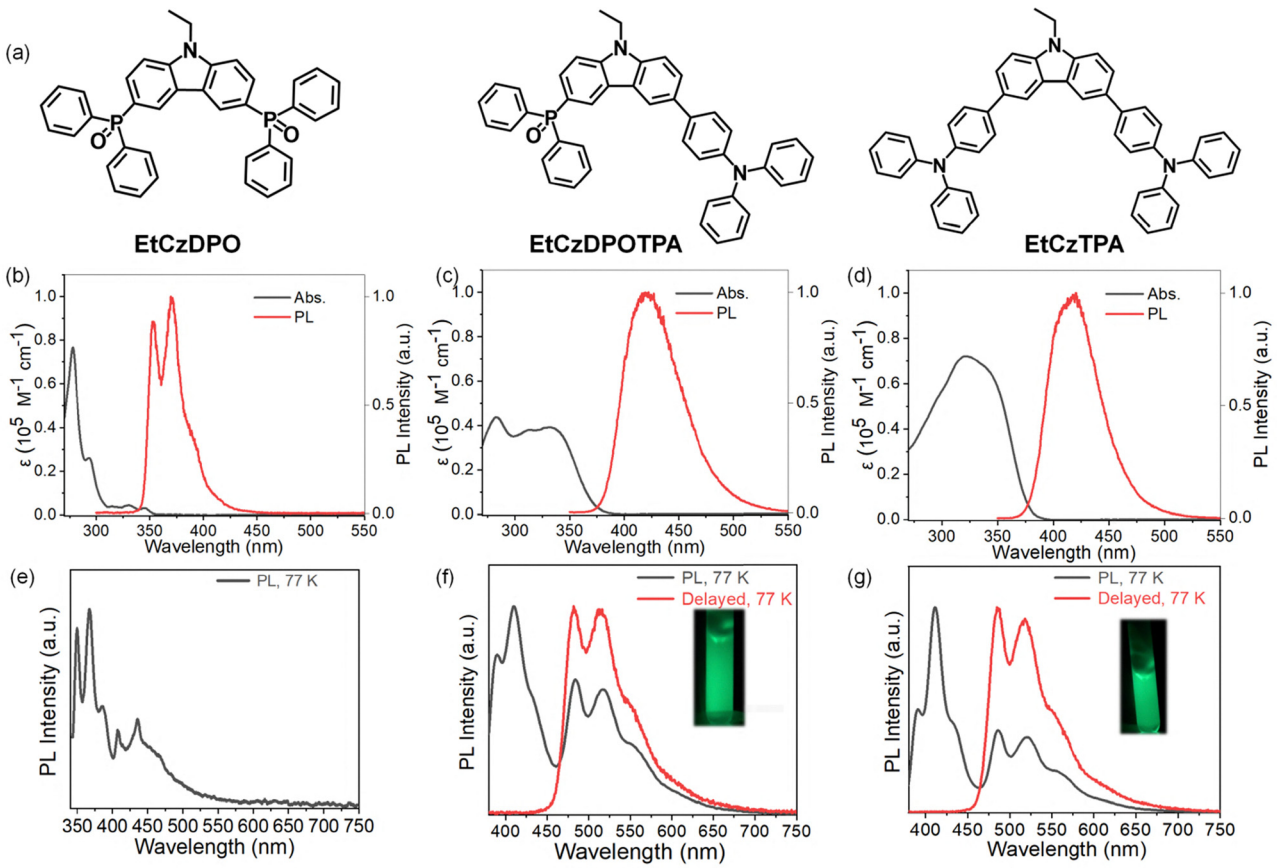

Fig. 2 (a) Chemical structures of EtCzDPO, EtCzDPOTPA and EtCzTPA. UV-Vis absorption and normalized steady-state PL spectra of (b) EtCzDPO, (c) EtCzDPOTPA and (d) EtCzTPA in a dilute DCM solution; steady-state PL spectra and delayed PL (delayed time = 8 ms) spectra for (e) EtCzDPO, (f) EtCzDPOTPA and (g) EtCzTPA. Inset: phosphorescent photographs at 77 K after UV excitation.

Additionally, host–guest interactions helped prevent aggregation-induced quenching of the guest molecules, ensuring that triplet excitons underwent radiative decay to produce phosphorescence at room temperature. Concurrently, the dynamic hydrogen-bonding networks within the elastomeric resins endowed the material with deformation capability up to 516.34%. Theoretical calculations further revealed that the synergistic EtCzTPADPO interaction reduced the singlet–triplet energy gap (ΔE_{ST}) to 0.54 eV and suppressed the exciton quenching during stretching through π–π confinement effects. This work pioneers the controllable 3D printing of phosphorescent elastomers, whose strain-luminescence synchronization properties offer groundbreaking solutions for flexible stress sensing and dynamic optical encoding.

Results and discussion

Firstly, the compounds EtCzDPO, EtCzTPADPO, and EtCzTPA were designed and synthesized, taking *N*-ethylcarbazole as the core component and incorporating TPA and TPO into its molecular skeleton. Detailed synthetic procedures for the target compounds are provided in Fig. S1 of the SI. The resulting compounds EtCzTPADPO, EtCzTPA, and EtCzDPO were comprehensively confirmed using ^{1}H NMR, ^{13}C NMR and high-resolution mass spectrometry (HRMS) (Fig. S2–S10). Subsequently, the photophysical properties of these materials in both solution and solid states were systematically investigated by their spectral characteristics. Dilute dichloromethane (DCM) solutions of EtCzDPO, EtCzTPADPO, and EtCzTPA were prepared at a concentration of 1.0×10^{-5} mol L^{-1}. Fig. 2b–d present the ultraviolet-visible (UV-vis) absorption and steady-state photoluminescence (PL) spectra of these compounds. The absorption peaks of EtCzDPO were located at 278, 293 and 331 nm; the peaks of EtCzTPADPO were located at 283 nm and 331 nm, and for EtCzTPA, a single peak was located at 321 nm. These absorptions were attributed to the typical π–π* transitions mixed with n–π* transitions.

The steady-state PL spectra revealed fluorescence emission peaks at 352 nm and 370 nm for EtCzDPO, at 422 nm for EtCzTPADPO, and at 421 nm for EtCzTPA. Notably, the emission peak of EtCzDPO in solution was blue-shifted compared with those of EtCzTPA and EtCzDPOTPA. In addition, we evaluated the steady-state PL spectra and delayed PL spectra of these compounds in 2-methyltetrahydrofuran (2-MeTHF) at a concentration of 1.0×10^{-5} mol L^{-1} at 77 K. As illustrated in Fig. 2e, under a 330 nm excitation, EtCzDPO showed structured emission characteristics at 77 K, with fluorescent emission peaks at 349 nm and 367 nm and phosphorescent emission peaks at 407 nm and 436 nm. However, due to the weak phosphorescence performance of this compound, its delayed PL spectra and phosphorescence images could not be captured at low temperatures. EtCzTPADPO exhibited structured PL emission features with peaks at approximately 409 nm, 483 nm, and 516 nm under a 365 nm excitation, while the delayed spectra displayed structured emission peaks at around 483 nm and 516 nm. The emission peak at 409 nm corresponded to fluorescence at low temperature, while the structured emission peaks at 483 nm and 516 nm were attributed to phosphorescence, with a green phosphorescent emission. At 77 K, the 2-MeTHF solvent formed a glassy state, suppressing non-radiative transitions of triplet excitons and resulting in prominent phosphorescence emission. Compared with EtCzTPADPO, EtCzTPA exhibited similar photophysical properties at low temperatures, a fluorescence emission peak at 411 nm and phosphorescence emission peaks at 485 nm and 518 nm, with green phosphorescence.

Fig. S11 shows the excitation spectra of EtCzDPO, EtCzTPADPO and EtCzTPA in their solid powder state. Results indicated that all the three compounds can be excited by UV light within the UV spectral region. Fig. S12–S14 present their steady-state PL spectra and time-resolved fluorescence decay curves in the powder state, respectively. EtCzDPO showed an emission peak at 390 nm with a fluorescence lifetime of 12.04 ns; EtCzTPADPO exhibited an emission peak at 440 nm with a fluorescence lifetime of 8.14 ns; and EtCzTPA exhibited an emission peak at 426 nm with a fluorescence lifetime of 3.95 ns. The fluorescence lifetimes of all the three compounds in the solid state were on the nanosecond scale, and no delayed luminescence was observed. These findings confirmed that EtCzDPO, EtCzTPADPO and EtCzTPA were typical fluorescent materials in their solid forms, with emission characteristics dominated by prompt fluorescence rather than phosphorescence. All the three EtCz derivatives exhibited fluorescence with PLQYs of 8.16% for EtCzDPO, 18.47% for EtCzTPADPO and 3.86% for EtCzTPA.

Although all the three compounds were typical fluorescent materials in their solid state, our experimental findings revealed that when doped into different polymer matrices, such as hydroxyethyl acrylate (HEA): acrylic acid (AA) photosensitive resin or isobornyl acrylate (IBOA): benzyl acrylate (BA) photosensitive elastic resin, EtCzTPA and EtCzTPADPO exhibited excellent RTP properties even at a doping amount of 0.1 wt%. Fig. 3 displays the photophysical properties of EtCzDPO, EtCzTPADPO and EtCzTPA doped in the HEA:AA resin. As shown in Fig. 3a–c, molecular vibrations in the excited state rendered the steady-state PL spectra with the characteristics of a structured emission, with the maximum emission peak at 368 nm for EtCzDPO@HEA:AA, 420 nm and 496 nm for EtCzTPADPO@HEA:AA and 426 nm and 502 nm for EtCzTPA@HEA:AA. Upon turning off the 365 nm UV light, the delayed PL spectra exhibited emission peaks at 407 nm and 440 nm for EtCzDPO@HEA:AA, 499 nm and 527 nm for EtCzTPADPO@HEA:AA and 493 nm and 523 nm for EtCzTPA@HEA:AA. As shown in Fig. 3d–f, time-resolved decay analysis revealed a phosphorescence lifetime of 46.75 ms for EtCzDPO@HEA:AA, 810 ms for EtCzTPADPO@HEA:AA and 630 ms for EtCzTPA@HEA:AA. Fig. S15 indicates fluorescence lifetimes of 8.81 ns for EtCzDPO@HEA:AA, 9.26 ns for EtCzTPADPO@HEA:AA and 4.54 ns for EtCzTPA@HEA:AA.

Delayed PL emissions originated from the phosphorescence emission of isolated molecules, which could be verified by the

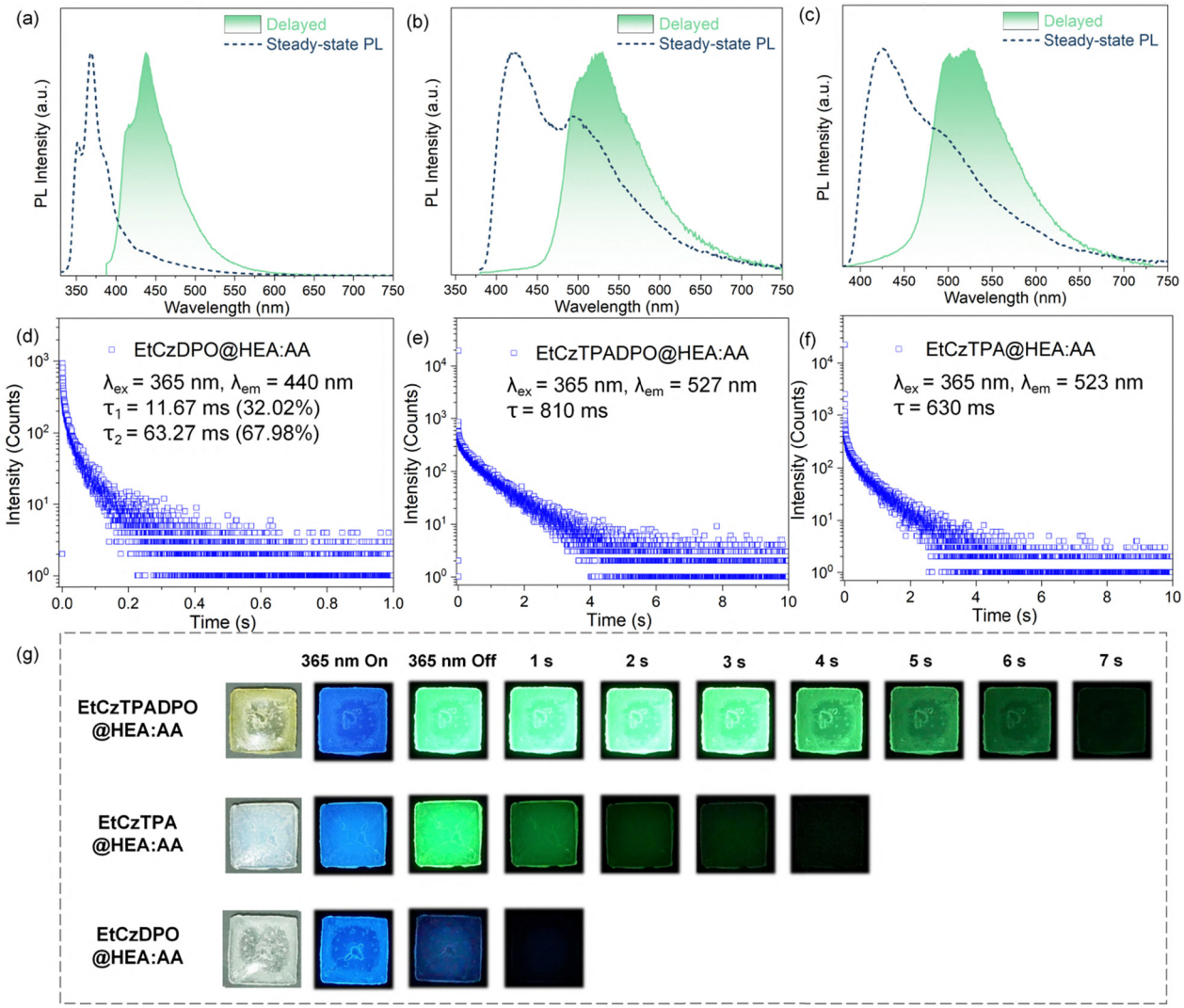

Fig. 3 Steady-state PL spectra and delayed PL (delayed time = 8 ms) spectra of (a) EtCzDPO@HEA:AA (b) EtCzTPADPO@HEA:AA and (c) EtCzTPA@HEA:AA under 297 K. (d) Time-resolved phosphorescence decay curve of (d) EtCzDPO@HEA:AA, (e) EtCzTPADPO@HEA:AA and (f) EtCzTPA@HEA:AA under 297 K (λ_{ex} = 365 nm). (g) Photographs of the EtCzDPO@HEA:AA, EtCzTPADPO@HEA:AA and EtCzTPA@HEA:AA films under UV excitation and after turning off the UV excitation (λ_{ex} = 365 nm).

phosphorescence spectra of these molecules in 2-MeTHF at 77 K. Within the HEA:AA resin, the guest molecules EtCzDPO, EtCzTPADPO and EtCzTPA formed strong intermolecular interactions with the polymer matrix, suppressing molecular vibrations in the excited state and giving rise to RTP. Indeed, Fig. 3g shows phosphorescent photographs of the three compounds doped in the HEA:AA photosensitive resin. Under UV excitation, the steady-state PL spectra of all the three compounds in the resin exhibited a blue emission. After turning off the UV light, EtCzTPADPO displayed a bright green afterglow emission that lasted about 7 s. In contrast, EtCzTPA exhibited a shorter afterglow duration of 4 s. The afterglow colors of both the compounds matched their phosphorescence colors observed in the glassy matrix of 2-MeTHF at 77 K. Therefore, this consistency further confirmed that the phosphorescence in the HEA:AA photosensitive resin originated from the lowest triplet excited state (T_1) of the single molecule. The RTP properties of EtCzDPO@HEA:AA were extremely weak, barely detectable even after the UV light was switched off, and could only be briefly captured by cameras. In contrast, the RTP performance of EtCzTPADPO within the HEA:AA resin surpassed those of the other two compounds, as shown in Fig. 3g.

Most currently reported host–guest organic RTP materials based on resin matrices exist as flexible thin films, where the rigid resin environment promotes phosphorescent emission from the lowest triplet excited state of the guest molecules. However, few elastomeric RTP materials compatible with digital light processing (DLP) 3D printing have been reported to date.[37–39] We developed an elastically deformable resin matrix using IBOA and BA, with aliphatic urethane diacrylate (AUD) as the crosslinker, and systematically investigated the RTP properties of the doped materials.

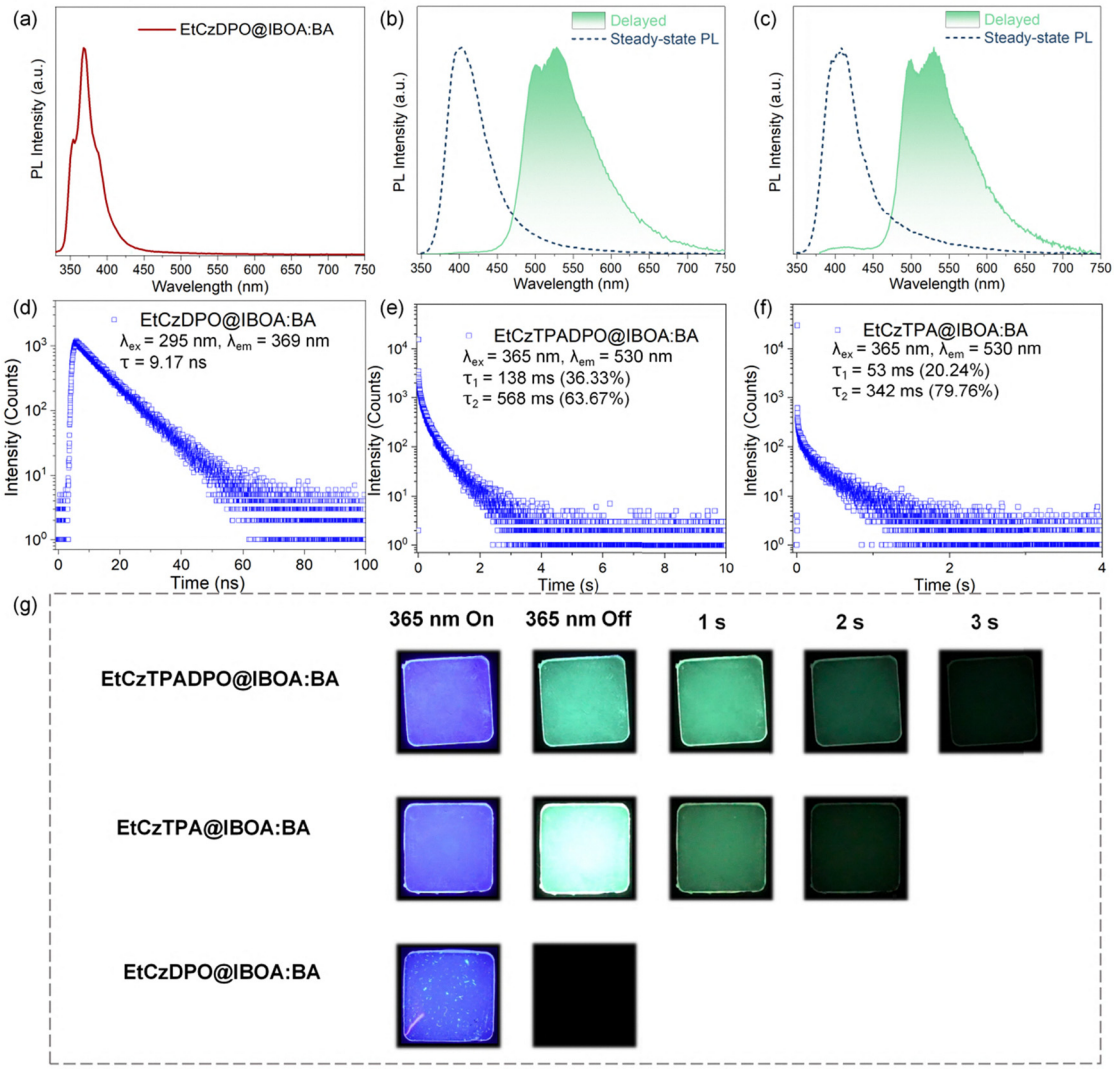

Fig. 4 Steady-state PL spectra (λ_{ex} = 310 nm) and delayed PL (λ_{ex} = 365 nm, delayed time = 8 ms) spectra of (a) EtCzDPO@IBOA:BA (b) EtCzTPADPO@IBOA:BA and (c) EtCzTPA@IBOA:BA under 297 K. Time-resolved decay curves of (d) EtCzDPO@IBOA:BA, (e) EtCzTPADPO@IBOA:BA and (f) EtCzTPA@IBOA:BA under 297 K. (g) Photographs of the EtCzDPO@IBOA:BA, EtCzTPADPO@IBOA:BA and EtCzTPA@IBOA:BA films under UV excitation and after turning off the UV excitation (λ_{ex} = 365 nm).

Fig. 4a shows the photophysical properties of EtCzDPO doped in the IBOA:BA matrix. EtCzDPO@IBOA:BA did not exhibit RTP in the IBOA:BA elastic resin. Upon excitation at 310 nm, its PL spectrum showed an emission peak at 369 nm with a lifetime of 9.17 ns. As noted earlier, its intrinsic phosphorescence was weak, and no phosphorescent emission was observed even in 2-MeTHF solution at 77 K. For EtCzTPADPO@IBOA:BA, the steady-state PL spectrum under UV excitation exhibited an emission peak at 400 nm. After the UV light was turned off, the delayed PL spectrum displayed peaks at 502 nm and 530 nm, as shown in Fig. 4b. EtCzTPA@IBOA:BA showed a steady-state PL emission peak at 422 nm under a 330 nm excitation. After the UV lamp was turned off, its delayed PL emission spectrum exhibited peaks at 499 nm and 530 nm, as shown in Fig. 4c. The delayed emission spectral peak profiles and emission maxima for both EtCzTPADPO and EtCzTPA in the IBOA:BA elastic resin closely matched those observed in their respective 77 K 2-MeTHF states. This indicates that the phosphorescence in the IBOA:BA elastic resin originates from the T_1 state of the guest molecules. Time-resolved decay curves revealed a fluorescence emission peak at 400 nm with a lifetime of 9.10 ns and a phosphorescence emission peak at 530 nm with a lifetime of 411.73 ms for EtCzTPADPO@IBOA:BA. However, the fluorescence emission peak at 422 nm exhibited a lifetime of 7.97 ns and the phosphorescence emission peak at 525 nm exhibited a lifetime of 283.75 ms for EtCzTPA@IBOA:BA. Compared with the photoluminescence quantum yield (PLQY) of 10.31% for EtCzTPADPO@IBOA:BA, EtCzTPA@IBOA:BA had a much lower PLQY (less than 1%), and this lower PLQY reflected its notably reduced RTP performance. Fig. 4g shows the RTP photographs of the three compounds doped in the IBOA:BA matrix. After UV excitation ceased, the resin

samples incorporating EtCzTPADPO and EtCzTPA exhibited RTP properties, while the sample with EtCzDPO@IBOA:BA failed to show any phosphorescence. Compared with their performance in the HEA:AA resin matrix, both EtCzTPADPO@IBOA:BA and EtCzTPA@IBOA:BA demonstrated significantly reduced RTP properties in the IBOA:BA elastic matrix. Within this elastic resin, EtCzTPADPO@IBOA:BA exhibited an RTP duration exceeding 3 s, while EtCzTPA@IBOA:BA showed a duration of 2 s.

To better illustrate the deformation capability of RTP elastomers, we conducted tensile tests on the EtCzTPADPO@IBOA:BA elastomer, as illustrated in Fig. S17. In the initial stage, stress increased linearly with strain, indicating elastic deformation and demonstrating that this elastomer can recover elastically during the initial stretching stage. After the strain exceeded 10%, the increase in stress slowed down as strain increased, and the elastomer began to undergo plastic deformation. Further increase in strain led to the elastomer reaching its tensile limit and subsequent fracture at strains exceeding 500%. The experimental results demonstrated that the elastomer exhibited an elongation at break of 516.34%, indicating excellent elastic performance. The EtCzTPADPO@IBOA:BA elastomer exhibited a deformation capacity of up to 516.34%, while the undoped elastomer showed a deformation capacity of only 379.58%. Compared with the pristine IBOA:BA elastomer, the EtCzTPADPO@IBOA:BA elastomer demonstrated distinctively enhanced deformation performance; this improvement was directly attributed to the incorporation of EtCzTPADPO molecules. Moreover, when the samples were stretched to 300% of their original length, as shown in Fig. S23, a decay in both the steady-state PL luminescence intensity and delayed PL luminescence intensity was observed, which was attributed to the reversible reconstruction of microstructures during dynamic deformation that tended to disrupt the excited-state energy transfer pathways of emitters, leading to luminescence decay.[36] Notably, the phosphorescent emission wavelength exhibited no significant shift during the deformation process induced by an external force. In addition, systematic characterizations of the elastomers were conducted, including infrared spectroscopy (IR), thermogravimetric analysis (TGA), and dynamic mechanical analysis (DMA), as shown in Fig. S18–S22.

To investigate the luminescence mechanism of RTP elastomers in detail, we performed density functional theory (DFT) and time-dependent DFT (TD-DFT) calculations based on the molecular geometries optimized at the B3LYP/6-311G* level for their ground states.[40–45] Notably, the molecules EtCzDPO, EtCzTPADPO, and EtCzTPA adopted a highly twisted conformation in their monomer states. In particular, for EtCzDPO, the electron-accepting DPO was surrounded by EtCz groups, resulting in a highly twisted structure. The twisted conformation effectively prevented the formation of coplanar packing, thereby suppressing the severe aggregation-caused quenching effect that is typical of polycyclic π-conjugated materials. This suppression was confirmed by our finding that all the three EtCz derivatives exhibited high fluorescence emission in their solid state, as illustrated above.

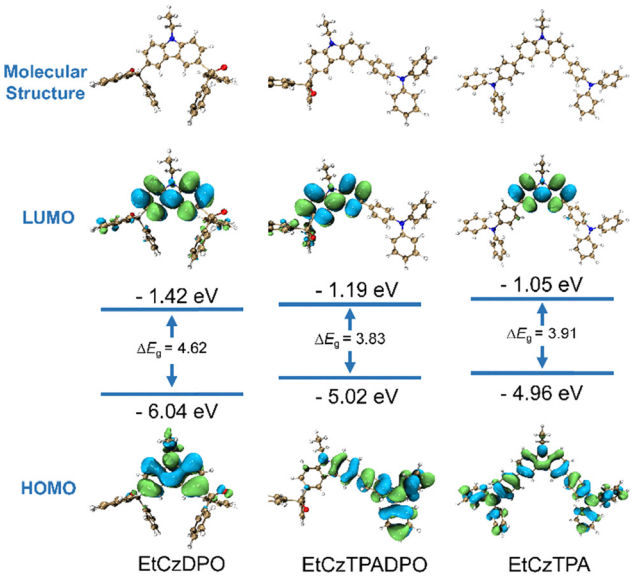

Fig. 5 HOMO and the LUMO density maps of EtCzDPO, EtCzTPADPO and EtCzTPA (calculated at the B3LYP/6-311G* level, isovalue = 0.02).

Furthermore, TD-DFT results revealed distinct electron density distributions for the highest occupied molecular orbitals (HOMOs) and the lowest unoccupied molecular orbitals (LUMOs) in these molecules (Fig. 5). In EtCzDPO, the HOMO and the LUMO were both highly localized on the EtCz moiety. This indicated that electronic excitation primarily occurred within the EtCz core unit. Concurrently, the DPO group did not participate in this process, demonstrating no contribution to either electron transfer or distribution of the frontier molecular orbitals. A relatively large HOMO–LUMO energy gap of 4.62 eV was exhibited by EtCzDPO as a result of this specificity in the electronic structure. EtCzTPADPO, on the other hand, displayed a different electron distribution pattern. Its HOMO orbital was mainly concentrated on the TPA group, while the EtCz part made a smaller but important contribution; its LUMO orbital was mostly spread over the EtCz part. Notably, the frontier orbital distribution and electron transfer processes were not affected by the DPO group present in this molecule. EtCzTPA's HOMO orbital was more spread out, covering both the TPA and EtCz groups, showing the shared electron characteristics between these parts. The LUMO orbital, on the other hand, was clearly focused on the EtCz region. EtCzTPADPO and EtCzTPA had similar HOMO–LUMO energy gaps of 3.83 eV and 3.91 eV, respectively, which were notably smaller than that of EtCzDPO. In EtCzTPADPO and EtCzDPO, the electron transition process involved a charge transfer from the TPA group to the EtCz group, while in EtCzDPO, the electron transition process only occurred within the EtCz group. Therefore, the charge transfer from the TPA group to the EtCz group was an important reason for the RTP phenomenon of EtCzTPADPO and EtCzTPA in the resin substrate.

Phosphorescence emission fundamentally correlated with the radiative transition from the T_1 state to the ground state (S_0) in the compounds. To gain deeper insights into the

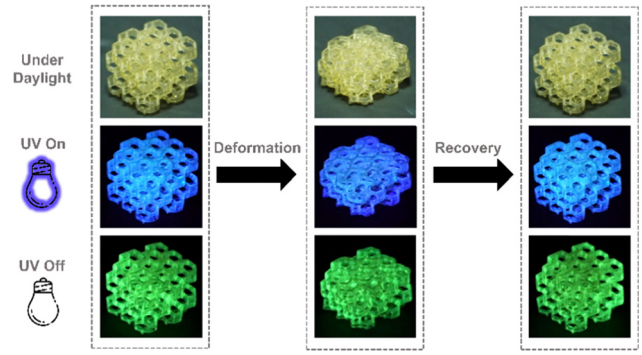

Fig. 6 Photographs of 3D RTP materials prepared by DLP 3D printing based on IBOA:BA resin under daylight, UV excitation and after switching off the UV excitation.

characteristics of EtCzDPO, EtCzTPADPO and EtCzTPA in the T_1 state, electron–hole isosurface plots corresponding to their respective $S_0 \rightarrow T_1$ transitions were evaluated (Fig. S24). Blue isosurfaces represented the spatial distribution of holes, while green isosurfaces represented the spatial distribution of excited electrons. These three-dimensional distribution models clearly revealed and compared the characteristics of the electronic transitions involved in the T_1 state excitation across different molecular systems. For EtCzTPADPO and EtCzTPA, holes were primarily localized on the TPA moiety, while electrons mainly distributed over the EtCz group, with partial extension to the phenyl rings of the triphenylamine unit adjacent to EtCz. This spatially separated charge distribution pattern unequivocally demonstrated that the T_1 in EtCzTPADPO and EtCzTPA exhibited pronounced ICT character. In contrast, for EtCzDPO, both electrons and holes were confined within the EtCz moiety, showing no discernible charge separation across distinct molecular fragments. This clearly indicates that the T_1 state of EtCzDPO represents a typical local excitation (LE).

To further elucidate the efficiency and pathways of intersystem crossing (ISC) between the excited states, we also analysed the detailed singlet (S_n) and triplet (T_n) energy levels of these compounds, as shown in Fig. S25–S27. The theoretically calculated lowest excited singlet state (S_1) and T_1 were 3.95/3.16 eV for EtCzDPO, 3.42/2.88 eV for EtCzTPADPO and 3.46/2.83 eV for EtCzTPA. In addition, we calculated the spin–orbit coupling (SOC) constants using the ORCA 4.0 program. It is proven that SOC constants (ξ) provide key insights into ISC rates. The ξ value for the $S_0 \rightarrow T_1$ transition in EtCzDPO was only 0.33 cm^{-1}, significantly lower than those of EtCzTPADPO (ξ = 0.68 cm^{-1}) and EtCzTPA (ξ = 0.64 cm^{-1}). This weaker SOC constant, combined with the larger ΔE_{ST} energy gap, resulted in weak intersystem crossing for EtCzDPO compared with the other two compounds. These results explained the weaker RTP observed for EtCzDPO in polymer matrices as efficient and rapid ISC is a prerequisite for strong phosphorescence emission. Conversely, the smaller ΔE_{ST} energy gaps and stronger SOC couplings enabled more efficient ISC pathways in EtCzTPADPO and EtCzTPA, which constitute key factors underlying their significant phosphorescence in resin matrices at room temperature. Corresponding excited-state energies and orbital transition compositions are detailed in Tables S1–S3.

Utilizing DLP 3D printing technology, we successfully fabricated 3D RTP flexible materials with elastic deformation capabilities by uniformly dispersing the highly efficient emitter EtCzTPADPO at a low doping concentration (0.1 wt%) within an IBOA:BA photosensitive resin matrix. As illustrated in Fig. 6, we printed a structurally sophisticated lattice framework model to demonstrate its practical formability. Upon deactivation of the ultraviolet excitation source, the printed 3D structure immediately exhibited a bright green phosphorescence originating from the T_1 of the doped EtCzTPADPO material.

When subjected to external forces, the printed structure underwent significant, visually discernible deformation. Remarkably, upon the removal of the forces, the structure spontaneously and fully recovered its initial configuration, demonstrating exceptional elasticity and reversible mechanical deformation characteristics. Critically, the phosphorescent emission properties, including intensity and wavelength, remained consistent throughout both the deformation process under external forces and after full recovery, with no observable alterations. This study pioneers the fabrication of 3D RTP materials with superior elastic deformation properties through DLP 3D printing technology. This achievement not only highlights the material's unique synergistic mechanical-optical properties but also lays the foundation for unlocking its potential applications in emerging fields like intelligent deformable structures.

Conclusions

In summary, this study proposes and validates an innovative, universal strategy that bridges molecular design and polymeric engineering, successfully achieving the precise fabrication of highly deformable RTP elastomers. These elastomers are perfectly compatible with advanced DLP 3D printing technology. By designing a class of functionalized EtCz derivatives and doping as phosphorescent chromophores into IBOA:BA resin, we achieved unification between extraordinary elastic deformability (fracture strain $>516\%$) and ultralong-lived RTP (phosphorescence lifetime $\tau \approx 412$ ms). Introduction of TPA and DPO units significantly reduced ΔE_{ST}, fundamentally ensuring efficient ISC. In addition, the weak interactions between the guest molecules and the polymer significantly suppresses the non-radiative transition of the triplet excitons. Critically, the phosphorescent emission wavelength showed no significant shift during both the deformation process under an external force and after full recovery. This approach effectively provides a new strategy for constructing 3D-printable elastomeric RTP materials.

Author contributions

Yuxin Xiao and Haodong Sun contributed equally. All authors contributed to the data analyses.

Conflicts of interest

There are no conflicts to declare.

Data availability

The data that support the findings of this study including synthesis and characterization and experimental details are available in the supplementary information (SI) of this article. See DOI: **https://doi.org/10.1039/d5qm00508f**.

Acknowledgements

The authors gratefully acknowledge the financial support from the NSF of China (62275217, T. Y.), the Natural Science Basic Research Programme of Shaanxi (2024JC-JCQN-51, T. Y.) and the Fundamental Research Funds for the Central Universities.

References

1 X. Dou, T. Zhu, Z. Wang, W. Sun, Y. Lai, K. Sui, Y. Tan, Y. Zhang and W. Z. Yuan, Color-Tunable, Excitation-Dependent, and Time-Dependent Afterglows from Pure Organic Amorphous Polymers, *Adv. Mater.*, 2020, **32**, 2004768.

2 Z. Yin, Z. Wu and B. Liu, Recent Advances in Impurity-Induced Room-Temperature Phosphorescence, *Adv. Mater.*, 2025, 2506549.

3 X. Luo, B. Tian, Y. Zhai, H. Guo, S. Liu, J. Li, S. Li, T. D. James and Z. Chen, Room-Temperature Phosphorescent Materials Derived from Natural Resources, *Nat. Rev. Chem.*, 2023, **7**, 800–812.

4 H. Zheng, Z. Zhang, S. Cai, Z. An and W. Huang, Enhancing Purely Organic Room Temperature Phosphorescence via Supramolecular Self-Assembly, *Adv. Mater.*, 2024, **36**, 2311922.

5 Y. Xiao, J. Li, Z. Song, J. Liao, M. Shen, T. Yu and W. Huang, 3D Printable Materials with Visible Light Triggered Photochromism and Room Temperature Phosphorescence, *J. Am. Chem. Soc.*, 2025, **147**, 20372.

6 X. Yang, G. I. N. Waterhouse, S. Lu and J. Yu, Recent Advances in the Design of Afterglow Materials: Mechanisms, Structural Regulation Strategies and Applications, *Chem. Soc. Rev.*, 2023, **52**, 8005.

7 J. Li, H. Zhou, H. Qiu, Y. Yan, X. Wang, Z. Gao and Z. Wang, Phosphorescent Carbon Dots: Intermolecular Interactions, Properties, and Applications, *Coord. Chem. Rev.*, 2024, **503**, 215642.

8 T. Li, N. Zhang, S. Zhao, M. Liu, K. Zhang, C. Zhang, J. Shu and T.-F. Yi, Long-lived Dynamic Room Temperature Phosphorescent Carbon Dots for Advanced Sensing and Bioimaging Applications, *Coord. Chem. Rev.*, 2024, **516**, 215987.

9 H. Zheng, Z. Zhang, S. Cai and W. Huang, Enhancing Purely Organic Room Temperature Phosphorescence *via* Supramolecular Self-Assembly, *Adv. Mater.*, 2024, **36**, 2311922.

10 G. Yin, J. Zhou, W. Lu, L. Li, D. Liu, M. Qi, B. Z. Tang, P. Théato and T. Chen, Targeting Compact and Ordered Emitters by Supramolecular Dynamic Interactions for High-performance Organic Ambient Phosphorescence, *Adv. Mater.*, 2024, **36**, 2311347.

11 X. Yan, H. Peng, Y. Xiang, J. Wang, L. Yu, Y. Tao, H. Li, W. Huang and R. Chen, Recent Advances on Host-Guest Material Systems toward Organic Room Temperature Phosphorescence, *Small*, 2022, **18**, 2104073.

12 L. Ma, Y. Liu, X. Jin, T. Jiang, L. Zhou, Q. Wang, H. Tian and X. Ma, Triplet Exciplex Mediated Multi-Color Ultra-Long Afterglow Mate-rials, *Angew. Chem., Int. Ed.*, 2025, **64**, e202500847.

13 X. Li, H. Kang, Y. Zhao, T. Chen, J. Zheng, L. Chen, B. Liu, Y. Yang and X. Liu, Mechanism of in Situ Confining Carbon Dots in Phthalamide Crystal for Room-Temperature Phosphorescence, *Mater. Chem. Front.*, 2025, **9**, 744–753.

14 X. Jiao, W. Zhang, J. Zhi, Y. Wang, M. Wang, Z. Liu and J. Li, Ultra-long organic RTP Host-Guest Doped Systems Based on Pure 4-(1H-imidazole-1-yl)methyl benzoate as Versatile Hosts, *Mater. Chem. Front.*, 2025, **9**, 1166–1173.

15 X. Li, H. Kang, Y. Zhao, T. Chen, J. Zheng, L. Chen, B. Liu, Y. Yang and X. Liu, Mechanism of in Situ Confining Carbon Dots in Phthalamide Crystal for Room-Temperature Phosphorescence, *Mater. Chem. Front.*, 2025, **9**, 1870–1881.

16 Z. Gong, Q. Cui, X. Nie, G. Zhang and B. Chen, Achieving Dual-Mode Long-Persistence Afterglow through an Aromatic Furan Organic Host-Guest System, *Mater. Chem. Front.*, 2025, **9**, 676–683.

17 H. Sun, X. Wei, Y. He, Y. Xiao, Y. Wu, Z. Xie and T. Yu, Regulation of Various Photo-Active UOPs in a Polymer Matrix by Tuning Intermolecular Charge Transfer, *Mater. Chem. Front.*, 2023, **7**, 3156–3163.

18 N. Gan, X. Zou, Y. Zhang, L. Gu and Z. An, Recent advances in multicolor organic room-temperature phosphorescence, *Appl. Phys. Rev.*, 2023, **10**, 021313.

19 S. Li, L. Fu, X. Xiao, H. Geng, Q. Liao, Y. Liao and H. Fu, Regulation of Thermally Activated Delayed Fluorescence to Room-Temperature Phosphorescent Emission Channels by Controlling the Excited-States Dynamics via J- and H-Aggregation, *Angew. Chem., Int. Ed.*, 2021, **60**, 18059.

20 J. Guo, C. Yang and Y. Zhao, Long-Lived Organic Room-Temperature Phosphorescence from Amorphous Polymer Systems, *Acc. Chem. Res.*, 2022, **55**, 1160.

21 L. Ai, W. Xiang, J. Xiao, H. Liu, J. Yu, L. Zhang, X. Wu, X. Qu and S. Lu, Tailored Fabrication of Full-Color Ultrastable Room-Temperature Phosphorescence Carbon Dots Composites with Unexpected Thermally Activated Delayed Fluorescence, *Adv. Mater.*, 2024, **36**, 2401220.

22 S. Guan, X. Chen, R. Yu, W. Xu, Z. Wu, Y. D. Suh, X. Liu and W. Huang, Opal-Inspired SiO2-Mediated Carbon Dot Doping Enables the Synthesis of Monodisperse Multifunctional Afterglow Nanocomposites for Advanced Information Encryption, *Angew. Chem., Int. Ed.*, 2024, **64**, e202415632.

23 Y. Ding, C. Yang, F. Gan, G. Zhang, C. Shen and H. Qiu, Ultrahigh-Temperature Long-Persistent Luminescence from

B2O3-Confined Polycyclic Aromatic Compounds, *J. Am. Chem. Soc.*, 2024, **146**, 25211.
24 D. Liu, Y. Song, H. Wang, Z. Zhou, Z. Liu and T. Wang, *J. Mol. Struct.*, 2024, **1313**, 138745.
25 J. Gu, W. Yuan, K. Chang, C. Zhong, Y. Yuan, J. Li, Y. Zhang, T. Deng, Y. Fan, L. Yuan, S. Liu, Y. Xu, S. Ling, C. Li, Z. Zhao, Q. Li, Z. Li and B. Z. Tang, Organic Materials with Ultrabright Phosphorescence at Room Temperature under Physiological Conditions for Bioimaging, *Angew. Chem., Int. Ed.*, 2025, **64**, e202415637.
26 L. Zhang, J. Li, Y. Zhang, W. Dai, Y. Zhang, X. Gao, M. Liu, H. Wu, X. Huang, Y. Lei and D. Ding, White Light-Excited Organic Room-Temperature Phosphorescence for Improved in Vivo Bioimaging, *Nat. Commun.*, 2025, **16**, 3970.
27 Z. He, J. Song, C. Li, Z. Huang, W. Liu and X. Ma, High-Performance Organic Ultralong Room Temperature Phosphorescence Based on Biomass Macrocycle, *Adv. Mater.*, 2025, **37**, 2418506.
28 Z. Yang, J. Qian, S. Zhao, Y. Lv, Z. Feng, S. Wang, H. He, S.-T. Zhang, H. Liu and B. Yang, Highly Sensitive Thianthrene Covalent Trimer Room-Temperature Phosphorescent Materials for Low-Concentration Oxygen Detection, *Angew. Chem., Int. Ed.*, 2025, e202424669.
29 X. Zhang, J. Liu, B. Chen, X. He, X. Li, P. Wei, P. F. Gao, G. Zhang, J. W. Y. Lam and B. Z. Tang, Highly Efficient and Persistent Room Temperature Phosphorescence from Cluster Exciton Enables Ultrasensitive off-on VOC Sensing, *Matter*, 2022, **5**, 3499–3512.
30 Y. Zhang, Q. Sun, L. Yue, Y. Wang, S. Cui, H. Zhang, S. Xue and W. Yang, Room Temperature Phosphorescent (RTP) Thermoplastic Elastomers with Dual and Variable RTP Emission, Photo-Patterning Memory Effect, and Dynamic Deformation RTP Response, *Adv. Sci.*, 2022, **9**, 2103402.
31 N. Li, S. Gu, Q. Wu and J. Wu, A General Strategy for Self-healing Elastomers with Ultralong Room-Temperature Phosphorescence, *Mater. Horiz.*, 2025, **12**, 5846.
32 J. Chen, Y. Zhang, S. Zhang, G. Liu, Q. Sun, S. Xue and W. Yang, Two-Phase Rubber-Plastic Matrices' Stabilization of Organic Room-Temperature Phosphorescence Afterglows Better than Plastic Matrix, *Small Structure*, 2023, **4**, 2300101.
33 G. Liu, S. Zhang, J. Chen, S. Xue, Q. Sun and W. Yang, Highly Elastic Full Hydrocarbon Ultralong RTP Polymers with Visible Light Excitable $S_0 \rightarrow T_1$ Population, *Adv. Opt. Mater.*, 2025, **13**, 2402847.
34 H. Zeng, H. Li, P. Zhen, J. Zhou, B. Xu, G. Shi, Y. Zhang, Z. Chi and C. Liu, Tuning Intramolecular Charge Transfer and Suppressing Rotations in Thianthrene Derivatives for Enhancement of Room-Temperature Phosphorescence, *Chem. Sci.*, 2025, **16**, 9169–9177.
35 M. Chen, B. Liu, J. Ren, C. Zhang, Z. Ren and Z.-H. Guan, Stretchable, Ultralong Room-Temperature Phosphorescence Poly(urethane-urea) Elastomer Resistant to Humidity and Heat, *Adv. Mater.*, 2025, 2504825.
36 K. J. Kalita, S. Mondal, C. M. Reddy and R. K. Vijayaraghavan, Temperature-Regulated Dual Phosphorescence and Mechanical Strain-Induced Luminescence Modulation in a Plastically Bendable and Twistable Organic Crystal, *Chem. Mater.*, 2023, **35**, 709–718.
37 R. Huang, Y. He, J. Wang, J. Zou, H. Wang, H. Sun, Y. Xiao, D. Zheng, J. Ma, T. Yu and W. Huang, Tunable Afterglow for Mechanical Self-Monitoring 3D Printing Structures, *Nat. Commun.*, 2024, **15**, 1596.
38 M. Che, B. Liu, J. Ren, C. Zhang, Z. Ren and Z.-H. Guan, Stretchable, Ultralong Room-Temperature Phosphorescence Poly(urethane-urea) Elastomer Resistant to Humidity and Heat, *Adv. Mater.*, 2025, **37**, 504825.
39 N. Li, S. Gu, Q. Wu and J. Wu, A General Strategy for Self-Healing Elastomers with Ultralong Room-Temperature Phosphorescence, *Mater. Horiz.*, 2025, **12**, 5846–5854.
40 H. Sun, Y. Xiao, Y. He, X. Wei, J. Zou, Y. Luo, Y. Wu, J. Zhao, V. Ka-Man Au and T. Yu, 3D Printable Organic Room-Temperature Phosphorescent Materials and Printed Real-Time Sensing and Display Devices, *Chem. Sci.*, 2025, **16**, 5299–5309.
41 C. Lee, W. Yang and R. G. Parr, Development of the Colle-Salvetti Correlation-Energy Formula into a Functional of the Electron Density, *Phys. Rev. B: Condens. Matter Mater. Phys.*, 1988, **37**, 785.
42 F. Neese, Software Update: the ORCA Program System, version 4.0, *Wiley Interdiscip. Rev.: Comput. Mol. Sci.*, 2018, **8**, e1327.
43 T. Lu and F. Chen, Multiwfn: A Multifunctional Wavefunction Analyzer, *J. Comput. Chem.*, 2012, **33**, 580.
44 Z. Liu, T. Lu and Q. Chen, An sp-hybridized All-carboatomic Ring, Cyclo[18]carbon: Electronic Structure, Electronic Spectrum, and Optical Nonlinearity, *Carbon*, 2020, **165**, 461.
45 W. Humphrey, A. Dalke and K. Schulten, VMD: Visual Molecular Dynamics, *J. Mol. Graph.*, 1996, **14**, 33.

